Hindawi Publishing Corporation
International Journal of Photoenergy
Volume 2012, Article ID 767905, 7 pages
doi:10.1155/2012/767905

Research Article

Synthesis and Characterization of Mn–C–Codoped TiO_2 Nanoparticles and Photocatalytic Degradation of Methyl Orange Dye under Sunlight Irradiation

Wei Xin, Duanwei Zhu, Guanglong Liu, Yumei Hua, and Wenbing Zhou

Laboratory of Plant Nutrition and Ecological Environment Research,
Centre for Microelement Research of Huazhong Agricultural University, Wuhan 430070, China

Correspondence should be addressed to Guanglong Liu, liugl0924@hotmail.com

Received 25 July 2012; Revised 5 September 2012; Accepted 5 September 2012

Academic Editor: Jiaguo Yu

Novel visible-light-active Mn–C–TiO_2 nanoparticles were synthesized by modified sol-gel method based on the self-assembly technique using polyoxyethylenes orbitan monooleate (Tween 80) as template and carbon precursor and manganese acetate as manganese precursor. The samples were characterized by XRD, FTIR, UV-vis diffuse reflectance, XPS, and laser particle size analysis. The XRD results showed that Mn–C–TiO_2 sample exhibited anatase phase and no other crystal phase was identified. High specific surface area, small crystallite size, and small particle size distribution could be obtained by manganese and carbon codoped and Mn–C–TiO_2 exhibited greater red shift in absorption edge of samples in visible region than that of C–TiO_2 and pure TiO_2. The photocatalytic activity of synthesized catalyst was evaluated by photocatalytic oxidation of methyl orange (MO) solution under the sunlight irradiation. The results showed that Mn–C–TiO_2 nanoparticles have higher activity than other samples under sunlight, which could be attributed to the high specific surface area, smaller particle size, and lower band gap energy.

1. Introduction

Photocatalytic degradation of toxic organic compounds has received a great attention for the past several years. Due to its strong oxidizing powder, being cost effective, and long-term stability against photo- and chemical corrosion, TiO_2 has been widely used in water purification technology [1–4]. However, the practical applications of TiO_2 are limited by its large band gap (3.2 eV), which can be only active under the UV light irradiation [5–7]. Therefore, several strategies have been developed to shift the optical sensitivity of TiO_2 from UV to the visible-light region for the efficient use of solar energy, such as element doping, metal deposition, surface sensitization, and couping of composite semiconductors [8]. Recently, C, N, F, S anion-doped TiO_2 photocatalysts that show a relatively high level of activity under visible-light irradiation have been reported [9]. These nonmetal elements have been proved to be beneficial dopants in the TiO_2 via mixing their p orbital of nonmetal with O 2p orbital to reduce the band gap energy of TiO_2. The doping of various transitional metal ions into TiO_2 could shift its optical absorption edge from UV into visible-light range, but a prominent change in TiO_2 band gap has not been observed [10]. This red shift in metal doped TiO_2 was attributed to the charge-transfer transition between the d electrons of the dopant and the conduction band (CB) of TiO_2 [11]. However, transition metal-doped TiO_2 suffers from some serious drawbacks, such as thermal instability and low quantum efficiency. In order to further improve the photocatalytic activity, codoped titania with double nonmetal [12, 13], metal-nonmetal elements [14–16], and double metal ions [17, 18] have attracted more attention. Some studies demonstrated that the codoping with transition metal and nonmetal elements could effectively modify the electronic structures of TiO_2 and shift its absorption edge to a low energy [16]. However, to the best of our knowledge, the preparation of manganese and carbon codoped titania has never been reported.

In addition, the structural properties of TiO_2, such as crystalline phase, crystallite size, surface area, and pore distribution, are important for its photocatalytic properties.

Recently, the use of self-assembly surfactant-based sol-gel methods has been reported as an effective approach to tailor-design the structural properties of TiO_2 nanoparticles from molecular precursors [19–22]. High surface area, high porosity, small crystal size, and narrow pore size distribution of TiO_2 could be obtained by a sol-gel method with hydrocarbon surfactants added. Specifically, these hydrocarbon surfactants can serve as a nonmetal doping precursor to increase the photocatalytic activity of TiO_2 under visible-light irradiation [23].

Therefore, in this work, nonionic surfactant Tween 80 was used as a pore template and carbon doping reagent in the sol-gel method to synthesize visible-light-active Mn–C–TiO_2 nanoparticles and the Mn–C–TiO_2 nanoparticles were described for their application in degrading organic dyes. Methyl orange (MeO), a typical azo dye, was used as the target pollutant in aqueous media to assess the photocatalytic activities of the Mn–C–TiO_2 nanoparticles. The capacities in the photocatalytic activities of the Mn–C–TiO_2 nanoparticles under sunlight irradiation were studied; the influence of calcinations temperature on the photocatalytic activities of composites and degradation pathway of pollutant were also discussed.

2. Materials and Methods

2.1. Synthesis of Visible-Light-Activated Mn–C–TiO_2 Nanoparticles. Mn–C–TiO_2 was prepared by the self-assembly surfactant-based sol-gel method under mild conditions as follow. A nonionic surfactant Tween 80 (T80, polyoxyethylenes orbitan monooleate, Guoyao Chemical Co.) was employed as the pore directing agent and carbon precursor in the modified sol-gel solution. 5 mL T80 was dissolved in 20 mL isopropyl alcohol (i–PrOH, 99.8%, Guoyao Chemical Co.) and then 3 mL titanium tetraisopropoxide (TTIP, 97%, Sigma-Aldrich) was added under vigorous stirring. Finally, 3 mL acetic acid (AcOH, Guoyao Chemical Co.) was added into the solution for the formation of water in the mixture. The sol-gel was aged at 65°C for 24 hrs. To synthesize particles, the sol was dried at room temperature for 3 hrs and then calcined at 400°C for 3 hrs. For comparison, pure titania, C-doped TiO_2, and Mn-doped TiO_2 were prepared though the same method, without adding the corresponding dopants.

2.2. Characterization of Synthesized Mn–C–TiO_2 Nanoparticles. To study the crystal structure and crystallinity of the Mn–C–TiO_2 nanoparticles, X-ray diffraction (XRD) analysis was performed on X'Pert PRO (D8 Advance) XRD diffractometer using Cu Kα (λ = 1.5406 Å) radiation. The particle diameter distribution of the samples was measured by particle diameter analyzer (Ankersmid Ltd.). Fourier transform infrared (FT-IR) spectroscopy was carried out using Thermo Scientific Nicolet 6700 spectrometer to detect the presence of carbon group on the samples. Measurement range was 4000–400 cm^{-1}, with a 4 cm^{-1} resolution, 0.475 cm^{-1}/s scan speed, and 32 scans. The technique applied was attenuated total reflectance (ATR) with an Avatar multibounce HATR accessory with ZnSe crystal at 45°. To investigate the light absorption and optical band gap of the synthesized TiO_2 nanoparticles, the UV-vis absorption spectra were obtained with a UV-vis spectrophotometer (Shimadzu 2450 PC) mounted with an integrating sphere accessory (ISR1200) using $BaSO_4$ as reference standard. An X-ray photoelectron spectroscope (XPS, PerkinElmer Model 5300) was employed to establish the nature of boron in the prepared manganese oxides by determining the binding energy with respect to Mn and C. The conditions of the equipment include a takeoff angle of 45° and vacuum pressure of 10^{-8} to 10^{-9} Torr. The binding energies were referenced to the C 1s peak at 284.6 eV.

2.3. Photocatalytic Evaluation with Methyl Orange under Visible Light. After synthesis and characterization, the Mn–C–TiO_2 nanoparticles were tested under sunlight irradiation for the degradation of methyl orange in water. Firstly, a particles suspension (0.5 g/L) solution was prepared and dispersed using an ultrasonicator (2510R-DH, Bransonic) for 24 h. Secondly, 10 μL methyl orange solution (500 mg/L) was transferred to a 50 mL particles suspension placed in reactor to achieve an initial concentration of 500 μg/L. Finally, 50 μL HNO_3 (0.05 mol L^{-1}) was added into the solution. During irradiation with two fluorescent lamps (20 W, Cole-Parmer) imitating sunlight, the reactor was sealed with parafilm and continuously mixed to minimize mass transfer limitations and the schematic diagram of photochemical reactor is depicted in Figure 1. A 0.2 mL sample was withdrawn at time 0, 1, 2, 3, 4, and 5 h. The photocatalyst was immediately removed from the samples after centrifugation. The progress of photocatalytic degradation was monitored through measuring the characteristic absorbance of the solution samples by a UV-760CRT UV-Vis spectrophotometer (Shanghai Precision and Scientific Instrument Co., Ltd). The characteristic absorbance peaks were shown in Figure 2. Due to the acidic condition, the characteristic absorbance peaks shift from 460 to 517 nm. So, λ_{max} = 517 nm was chosen to measure the content of methyl orange left in the sample.

3. Results and Discussion

3.1. X-Ray Diffraction. The photocatalytic activity of catalyst was greatly affected by its crystal structure and crystal phase [24]. Generally, the anatase phase is reported with high photocatalytic activity. Therefore, the crystal structure and crystal phase characterization of pure TiO_2 is investigated by XRD. The XRD patterns of samples are shown in Figure 3. In TiO_2 sample, rutile phase was detected; however, only anatase TiO_2 crystal phase could be identified in C–TiO_2 and Mn–C–TiO_2 samples and no other dopant related crystal phases could be resolved. The intensity of anatase diffraction peaks for the Mn–C–TiO_2 and C–TiO_2 samples decreased slightly as the T80 adding. This is probably due to the fact that the T80 suppresses the hydrolysis of titanium alkoxide and the rapid crystallization of the TiO_2 particles by adsorbing on the TiO_2 particle surface [25]. The average crystalline size calculated by applying the Scherrer formula on

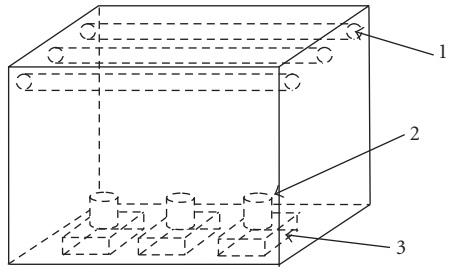

Figure 1: Schematic diagram of photocatalytic reactor. 1: fluorescent tube (20 W); 2: quartz petri dishes (diameter: 4.5 cm; height: 12 cm); 3: magnetic stirrers.

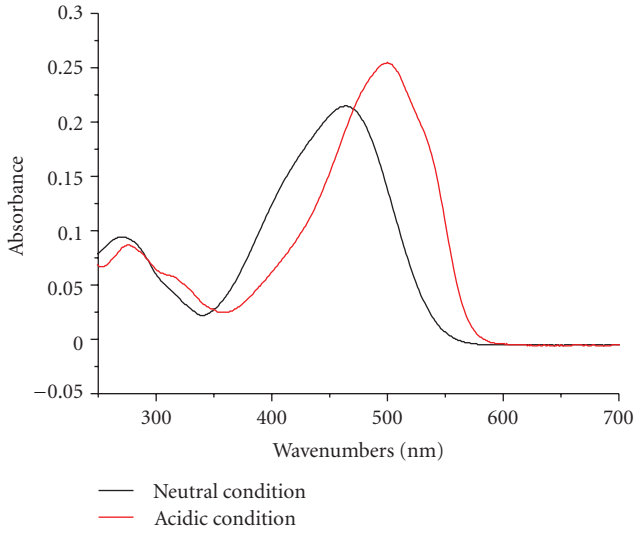

Figure 2: UV-vis spectra of methyl orange under neutral condition and acidic condition.

the anatase (101) diffraction peak was 37.23, 16.22, and 16.37 nm for the pure TiO_2, C–TiO_2, and Mn–C–TiO_2 samples, respectively, which is decreased as the surfactant used, since surfactant reduces the rate of titanium alkoxide hydrolysis and condensation of TiO_2 leading to smaller crystal size [26].

3.2. Particle Size Distribution. The particle diameter distribution of the pure TiO_2, C–TiO_2, and Mn–C–TiO_2 samples is shown in Figure 4. From the laser particle size analysis results, the mean particle diameter of the pure TiO_2, C–TiO_2, and Mn–C–TiO_2 samples is 80.46, 50.82, and 31.22 μm, respectively. The mean particle diameter also decreased with carbon and manganese doped, which may be associated with the role of the surfactant in the preparation process that decreases the polarity of titanium oxide (titania) and reduces the aggregation of the particles [26].

3.3. FT-IR Analysis. To give additional evidence and further to confirm the doping of manganese and carbon, FT-IR characterizations were performed. The infrared spectroscopy of pure TiO_2, C–TiO_2, and Mn–C–TiO_2 samples are presented

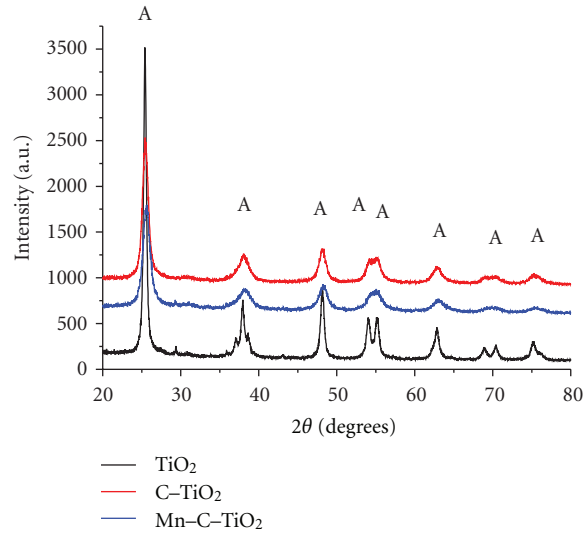

Figure 3: XRD patterns of as-prepared samples (A: anatase).

in Figure 5. The bands at 1640 cm^{-1} and the wide bands at 3100–3700 cm^{-1} is resultant from O–H stretching of adsorbed water molecules and the surface hydroxyl groups on TiO_2 have been recognized to play an important role in the photocatalytic process, as these groups can inhibit the recombination of photogeneration charges and interact with photogenerated holes to product reactive oxygen species [27]. The bands at 2330 cm^{-1} are assigned to the stretching vibrations of the C=O bonds. Compared with pure TiO_2 sample, we can infer that the C=O bonds in the C–TiO_2 and Mn–C–TiO_2 samples could be attributed to the T80 used in the sol. In the region below 1000 cm^{-1}, this peak was ascribed to absorption bands of Mn–O, which could be inferred that some manganese oxide may appear on the surface of TiO_2 nanoparticles [28].

3.4. UV-Vis Diffuse Reflectance Spectra. It is well know that the photocatalytic activity of a semiconductor is related to its band gap structure. Figure 6 shows the UV-vis absorption spectra of the pure TiO_2, C–TiO_2, and Mn–C–TiO_2 samples. The typical onset of absorption near 380 nm can be assigned to the intrinsic band gap absorption of TiO_2 [29]. It can be seen that there is a significant shift in the onset absorption toward the higher wavelength for the Mn–C–TiO_2 and C–TiO_2 sample. Specially, the codoped sample exhibits a greater red shift than C–TiO_2 sample which demonstrated that Mn–C–TiO_2 sample can greatly improve the absorption of visible light. The reason may be due to the new electronic state in the middle of the TiO_2 band gap, charge-transfer transition between the d electrons of the dopant and the CB of TiO_2, and the narrowed band gap resulted by C-doping, allowing visible light absorption [30]. It has been reported that nonmetal elements could reduce the band gap energy of TiO_2 by mixing their p orbital of nonmetal with O 2p orbital and the doping of various transitional metal ions into TiO_2 could shift its optical absorption edge from UV to visible-light range without a prominent change in TiO_2 band

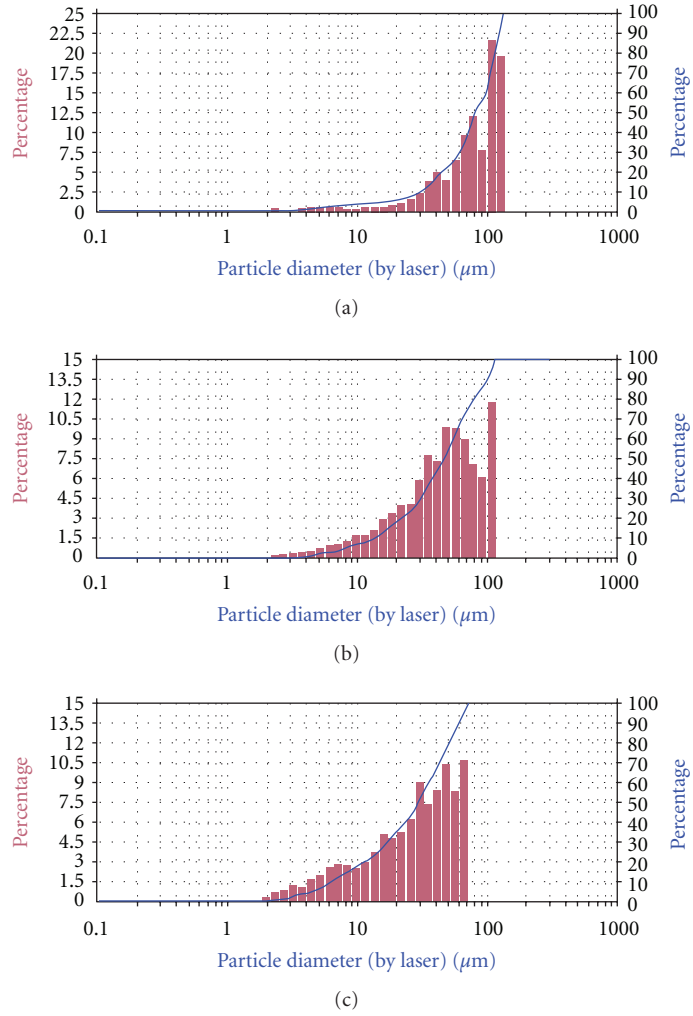

Figure 4: Particle size distribution of TiO_2, C–TiO_2, and Mn–C–TiO_2.

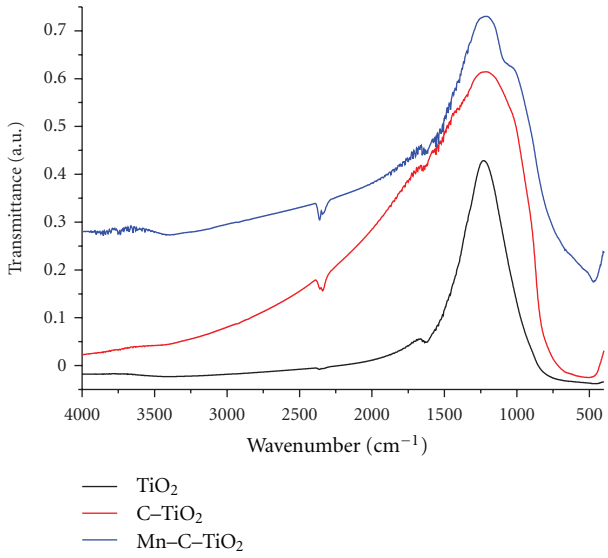

Figure 5: FT-IR spectra of TiO_2, C–TiO_2, and Mn–C–TiO_2.

gap [31]. However, the Mn–C doping TiO_2 samples showed smallest band gap energy in three kinds of samples shown in Figure 6(b). The direct band gap energy of Mn–C–TiO_2 sample was 2.6 eV, smaller than C–TiO_2 sample (3.0 eV) and pure TiO_2 sample (anatase, Ca. 3.2 eV). This result further approved the substitution of crystal lattice O or Ti to dopant species The enhanced ability to absorb visible light makes this Mn–C–TiO_2 an effective photocatalyst for solar-driven application.

3.5. XPS Spectra. XPS spectra showed further information on the structure of Mn–C–TiO_2. Figure 7(a) shows the high-resolution Mn 2p XPS spectra of Mn–C–TiO_2. The two Mn 2p peaks at the binding energy of 640.5 and 653.0 eV indicate the existence of MnO_2. The C 1s XPS spectra of Mn–C–TiO_2 were shown in Figure 7(b). Three broad but well-separated peaks were observed in the C 1s binding region at 281.3, 284.6, and 288.2 eV for the as-synthesized carbon-doped titania, but only one peak at 284.6 eV for pure titania (data not shown), which arises from adventitious elemental

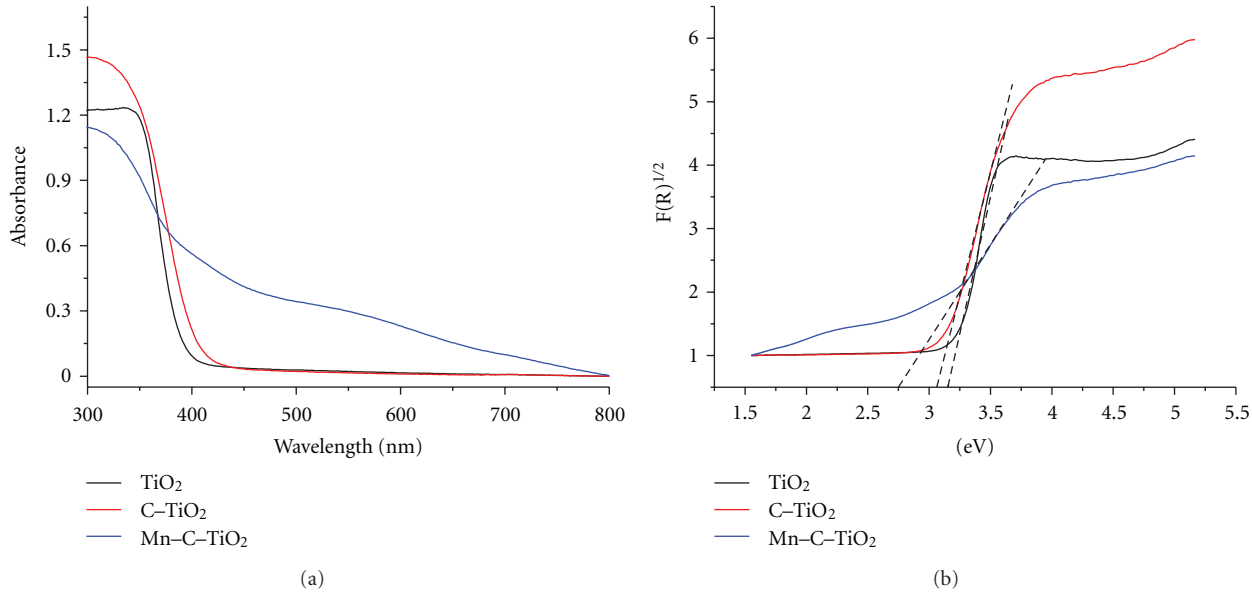

Figure 6: Optical properties of TiO_2, C–TiO_2, and Mn–C–TiO_2.

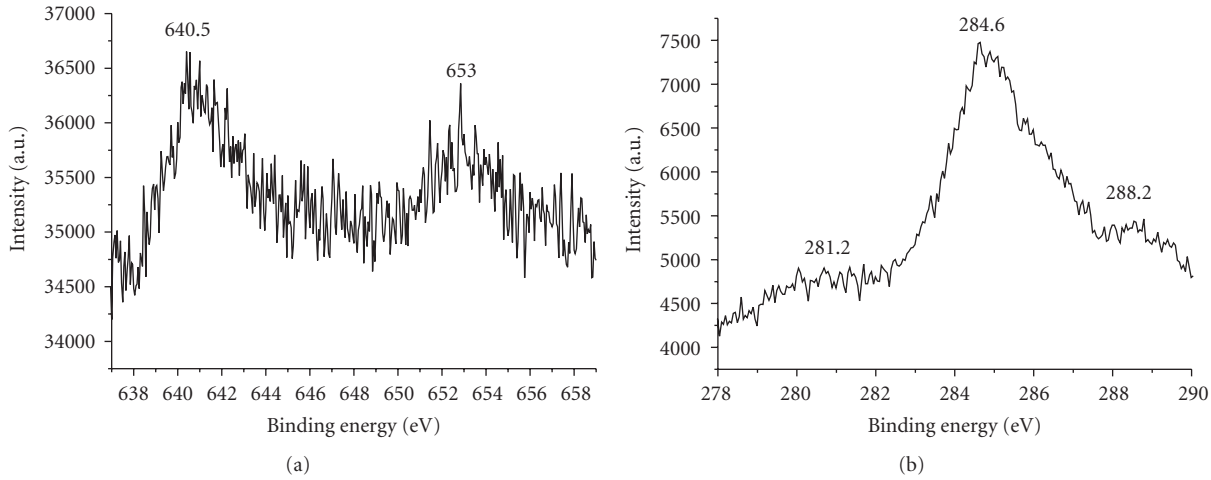

Figure 7: XPS spectra of codoped TiO_2 nanotube arrays. (a) A spectrum of Mn 2p; (b) a spectrum of C 1s.

carbon. The peak at the lower binding energy has been accordingly assigned to the formation of Ti–C bonds in C–TiO_2 in the previous reported [32]. The highest C 1s energy peak at 288.2 has been accordingly interpreted as the distinct feature of C–O bond formation in C–TiO_2 that in principle arises from interstitial and/or substitutional (for Ti) C atoms, while the underlying carbonate species have been considered as the source of the extended optical absorption tail of C–TiO_2 in the visible range [32]. In the present case, the coexistence of the 281.3 and 288.2 eV C 1s peaks corresponding to the binding energies of Ti–C and C–O bonds indicates both the presence of interstitial C atoms as well as carbon substitution for O and Ti atoms in the titania lattice [33].

3.6. Photocatalytic Activity of Samples in Photodegradation of Mn–C–TiO_2. To evaluate and compare the visible-light photocatalytic activity of the Mn–C–TiO_2 sample, the reactions of methyl orange degradation were preformed as photoreaction probes under the sunlight irradiation. In order to identify possible losses of methyl orange in the reactor system, control experiments without catalyst added were preformed. The course of methyl orange photocatalytic degradation used as catalyst pure TiO_2, C–TiO_2, and Mn–C–TiO_2 as well as control experiment is given in Figure 8. It was found that no obvious methyl orange loss was observed in control experiment which confirmed that the methyl orange was stable in our experiment. When adding the synthesized catalyst, it was seen from the figure that Mn–C–TiO_2 sample

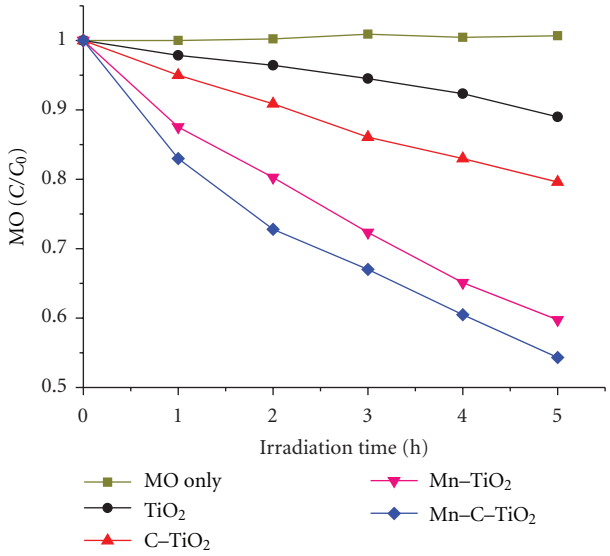

Figure 8: Photocatalytic degradation of MO with as-prepared samples.

exhibited higher photoactivity than that of pure TiO_2 and C–TiO_2 samples after 5 h irradiation under the sunlight. For pure TiO_2 sample, the degradation phenomenon could be attributed to the adsorption and photocatalytic degradation induced by trace UV light in the reaction system. In the Mn–C–TiO_2 system, the excellent photocatalytic activity could partially be due to its high specific surface area, smaller crystallite size, and lower band gap energy.

4. Conclusions

The manganese and carbon codoped TiO_2 nanoparticles as a novel catalyst were successfully prepared by surfactant-based sol-gel methods under mild conditions. For comparison, carbon doped TiO_2 and pure TiO_2 were also prepared by the same method without adding the corresponding dopants. Detailed characterization of the materials physicochemical properties by XRD and laser particle size analysis showed that the C–TiO_2 nanomaterials crystallize in the anatase phase with high specific surface area and small particle size distribution. Significant shift of the optical absorption edge toward the visible region was detected for the Mn–C–TiO_2 nanoparticles and much higher photocatalytic activity than that of C–TiO_2 and pure TiO_2 for methyl orange degradation in water was demonstrated under sunlight irradiation.

Acknowledgments

This paper was financially supported by the National Natural Science Foundation of China (40973056), Fundamental Research Funds for the Central Universities (2011PY114), Natural Science Foundation of Hubei Province of China (2011CDB135), and Specialized Research Fund for the Doctoral Program of Higher Education of China (20100146110020).

References

[1] A. Naldoni, M. Allieta, S. Santangelo et al., "Effect of nature and location of defects on bandgap narrowing in black TiO_2 nanoparticles," *Journal of the American Chemical Society*, vol. 134, no. 18, pp. 7600–7603, 2012.

[2] J. Yu, M. Jaroniec, and G. Lu, "TiO_2 photocatalytic materials," *International Journal of Photoenergy*, vol. 2012, Article ID 206183, 5 pages, 2012.

[3] S. K. Choi, S. Kim, S. K. Lim, and H. Park, "Photocatalytic comparison of TiO_2 nanoparticles and electrospun TiO_2 nanofibers: effects of mesoporosity and interparticle charge transfer," *Journal of Physical Chemistry C*, vol. 114, no. 39, pp. 16475–16480, 2010.

[4] L. Yang, X. Jiang, W. Ruan et al., "Charge-transfer-induced surface-enhanced raman scattering on Ag-TiO_2 nanocomposites," *Journal of Physical Chemistry C*, vol. 113, no. 36, pp. 16226–16231, 2009.

[5] J. Qian, G. Cui, M. Jing, Y. Wang, M. Zhang, and J. Yang, "Hydrothermal synthesis of nitrogen-doped titanium dioxide and evaluation of its visible light photocatalytic activity," *International Journal of Photoenergy*, vol. 2012, Article ID 198497, 6 pages, 2012.

[6] M. Zhou, J. Zhang, B. Cheng, and H. Yu, "Enhancement of visible-light photocatalytic activity of mesoporous Au-TiO_2 nanocomposites by surface plasmon resonance," *International Journal of Photoenergy*, vol. 2012, Article ID 532843, 10 pages, 2012.

[7] M. Zhou and J. Yu, "Preparation and enhanced daylight-induced photocatalytic activity of C,N,S-tridoped titanium dioxide powders," *Journal of Hazardous Materials*, vol. 152, no. 3, pp. 1229–1236, 2008.

[8] S. G. Kumar and L. G. Devi, "Review on modified TiO_2 photocatalysis under UV/visible light: selected results and related mechanisms on interfacial charge carrier transfer dynamics," *The Journal of Physical Chemistry A*, vol. 115, no. 46, pp. 13211–13241, 2011.

[9] X. Cheng, X. Yu, Z. Xing, and L. Yang, "Enhanced visible light photocatalytic activity of mesoporous anatase TiO_2 codoped with nitrogen and chlorine," *International Journal of Photoenergy*, vol. 2012, Article ID 593245, 6 pages, 2012.

[10] V. C. Papadimitriou, V. G. Stefanopoulos, M. N. Romanias et al., "Determination of photo-catalytic activity of un-doped and Mn-doped TiO_2 anatase powders on acetaldehyde under UV and visible light," *Thin Solid Films*, vol. 520, no. 4, pp. 1195–1201, 2011.

[11] J. C. S. Wu and C. H. Chen, "A visible-light response vanadium-doped titania nanocatalyst by sol-gel method," *Journal of Photochemistry and Photobiology A*, vol. 163, no. 3, pp. 509–515, 2004.

[12] X. Li, R. Xiong, and G. Wei, "S-N Co-doped TiO_2 photocatalysts with visible-light activity prepared by sol-gel method," *Catalysis Letters*, vol. 125, no. 1-2, pp. 104–109, 2008.

[13] L. Lin, R. Y. Zheng, J. L. Xie, Y. X. Zhu, and Y. C. Xie, "Synthesis and characterization of phosphor and nitrogen co-doped titania," *Applied Catalysis B*, vol. 76, no. 1-2, pp. 196–202, 2007.

[14] C. Liu, X. Tang, C. Mo, and Z. Qiang, "Characterization and activity of visible-light-driven TiO_2 photocatalyst codoped with nitrogen and cerium," *Journal of Solid State Chemistry*, vol. 181, no. 4, pp. 913–919, 2008.

[15] K. Obata, H. Irie, and K. Hashimoto, "Enhanced photocatalytic activities of Ta, N co-doped TiO_2 thin films under visible light," *Chemical Physics*, vol. 339, no. 1–3, pp. 124–132, 2007.

[16] X. Yang, C. Cao, K. Hohn et al., "Highly visible-light active C- and V-doped TiO_2 for degradation of acetaldehyde," *Journal of Catalysis*, vol. 252, no. 2, pp. 296–302, 2007.

[17] D. R. Zhang, Y. H. Kim, and Y. S. Kang, "Synthesis and characterization of nanoparticle of TiO_2 co-doped with Sc^{3+} and V^{5+} ions," *Current Applied Physics*, vol. 6, no. 4, pp. 801–804, 2006.

[18] R. Khan, S. W. Kim, T. J. Kim, and C. M. Nam, "Comparative study of the photocatalytic performance of boron-iron Co-doped and boron-doped TiO_2 nanoparticles," *Materials Chemistry and Physics*, vol. 112, no. 1, pp. 167–172, 2008.

[19] H. Choi, E. Stathatos, and D. D. Dionysiou, "Photocatalytic TiO_2 films and membranes for the development of efficient wastewater treatment and reuse systems," *Desalination*, vol. 202, no. 1–3, pp. 199–206, 2007.

[20] Y. Chen, E. Stathatos, and D. D. Dionysiou, "Microstructure characterization and photocatalytic activity of mesoporous TiO_2 films with ultrafine anatase nanocrystallites," *Surface and Coatings Technology*, vol. 202, no. 10, pp. 1944–1950, 2008.

[21] H. Choi, E. Stathatos, and D. D. Dionysiou, "Synthesis of nanocrystalline photocatalytic TiO_2 thin films and particles using sol-gel method modified with nonionic surfactants," *Thin Solid Films*, vol. 510, no. 1-2, pp. 107–114, 2006.

[22] H. Choi, A. C. Sofranko, and D. D. Dionysiou, "Nanocrystalline TiO_2 photocatalytic membranes with a hierarchical mesoporous multilayer structure: synthesis, characterization, and multifunction," *Advanced Functional Materials*, vol. 16, no. 8, pp. 1067–1074, 2006.

[23] H. Choi, M. G. Antoniou, M. Pelaez, A. A. De La Cruz, J. A. Shoemaker, and D. D. Dionysiou, "Mesoporous nitrogen-doped TiO_2 for the photocatalytic destruction of the cyanobacterial toxin microcystin-LR under visible light irradiation," *Environmental Science and Technology*, vol. 41, no. 21, pp. 7530–7535, 2007.

[24] M. Pelaez, A. A. de la Cruz, E. Stathatos, P. Falaras, and D. D. Dionysiou, "Visible light-activated N-F-codoped TiO_2 nanoparticles for the photocatalytic degradation of microcystin-LR in water," *Catalysis Today*, vol. 144, no. 1-2, pp. 19–25, 2009.

[25] P. D. Cozzoli, A. Kornowski, and H. Weller, "Low-temperature synthesis of soluble and processable organic-capped anatase TiO_2 nanorods," *Journal of the American Chemical Society*, vol. 125, no. 47, pp. 14539–14548, 2003.

[26] G. Liu, C. Han, M. Pelaez et al., "Synthesis, characterization and photocatalytic evaluation of visible light-activated C-doped TiO_2," *Nanotechnology*, vol. 23, 10 pages, 2012.

[27] Y. Huang, W. K. Ho, S. C. Lee, L. Z. Zhang, X. X. Fan, and Z. G. Zou, "Synthesis, characterization and photocatalytic evaluation of visible light-activated C-doped TiO_2," *Langmuir*, vol. 24, no. 7, pp. 3510–3516, 2008.

[28] G. Liu, S. Liao, D. Zhu, J. Cui, and W. Zhou, "Solid-phase photocatalytic degradation of polyethylene film with manganese oxide OMS-2," *Solid State Sciences*, vol. 13, no. 1, pp. 88–94, 2011.

[29] A. I. Kontos, A. G. Kontos, Y. S. Raptis, and P. Falaras, "Nitrogen modified nanostructured titania: electronic, structural and visible-light photocatalytic properties," *Physica Status Solidi*, vol. 2, no. 2, pp. 83–85, 2008.

[30] M. Hamadanian, A. Reisi-Vanani, M. Behpour, and A. S. Esmaeily, "Synthesis and characterization of Fe, S-codoped TiO_2 nanoparticles: application in degradation of organic water pollutants," *Desalination*, vol. 281, pp. 319–324, 2011.

[31] S. Liu, J. Yu, B. Cheng, and M. Jaroniec, "Fluorinated semiconductor photocatalysts: tunable synthesis and unique properties," *Advances in Colloid and Interface Science*, vol. 173, pp. 35–53, 2012.

[32] J. Yu, G. Dai, Q. Xiang, and M. Jaroniec, "Fabrication and enhanced visible-light photocatalytic activity of carbon self-doped TiO_2 sheets with exposed {001} facets," *Journal of Materials Chemistry*, vol. 21, no. 4, pp. 1049–1057, 2011.

[33] G. Liu, C. Han, M. Pelaez et al., "Synthesis, characterization and photocatalytic evaluation of visible light-activated C-doped TiO_2," *Nanotechnology*, vol. 23, no. 29, Article ID 294003, 10 pages, 2012.